

## Induction of Stemlike Cells with Fibrogenic Properties by Carbon Nanotubes and Its Role in Fibrogenesis

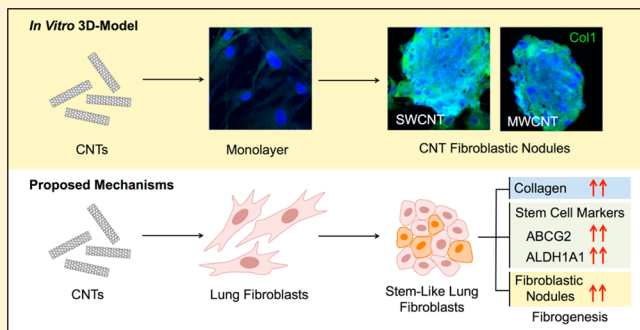
Sudjit Luanpitpong,<sup>†,‡</sup> Liying Wang,<sup>†</sup> Amruta Manke,<sup>†</sup> Karen H. Martin,<sup>§</sup> Amanda Gatesman Ammer,<sup>§</sup> Vincent Castranova,<sup>†</sup> Yong Yang,<sup>||</sup> and Yon Rojansakul\*,<sup>†,‡</sup>

<sup>†</sup>Pharmaceutical and Pharmacological Sciences Program, <sup>‡</sup>Mary Babb Randolph Cancer Center, <sup>§</sup>Animal Models and Imaging Facility, and <sup>||</sup>Department of Chemical Engineering, West Virginia University, Morgantown, West Virginia 26506, United States

<sup>†</sup>Pathology and Physiology Research Branch, National Institute for Occupational Safety and Health, Morgantown, West Virginia 26505, United States

### Supporting Information

**ABSTRACT:** We developed a three-dimensional fibroblastic nodule model for fibrogenicity testing of nanomaterials and investigated the role of fibroblast stemlike cells (FSCs) in the fibrogenic process. We showed that carbon nanotubes (CNTs) induced fibroblastic nodule formation in primary human lung fibroblast cultures resembling the fibroblastic foci in clinical fibrosis and promoted FSCs that are highly fibrogenic and a potential driving force of fibrogenesis. This study provides a predictive 3D model and mechanistic insight on CNT fibrogenesis.



**KEYWORDS:** Carbon nanotubes, lung fibrosis, stem-like fibroblasts, fibroblastic nodules, side population

Engineered nanomaterials have increasingly been used for a wide array of applications in the fields as diverse as electronics, energy, waste treatment, consumer products, and medicine. Carbon nanotubes (CNTs) are a major class of engineered nanomaterials possessing unique mechanical, electrical, and thermal properties and are being produced on a massive scale.<sup>1,2</sup> The global market for CNTs is estimated to reach a trillion dollars in the next decade<sup>3</sup> with their use affecting millions of workers and users. Because of their rapid rise in production and utility, it is important to determine their unintended consequences, especially on human health and the environment. CNTs can come into contact with human body mainly via inhalation and the major target organ of exposure is the lung. Animal exposure studies have shown that inhaled or instilled CNTs rapidly entered the alveolar interstitial space to induce progressive interstitial lung fibrosis without causing persistent lung injury and inflammation.<sup>4–6</sup> Subsequent in vitro studies showed that CNTs can directly interact with lung fibroblasts and stimulate their growth and production of collagen extracellular matrix (ECM) leading to fibrosis.<sup>7,8</sup> These effects of CNTs present an enormous health concern and a great challenge to the assessment of potential health hazards of CNTs since lung fibrosis is a fatal and incurable disease with no known effective treatment.

Currently, rodent models are the gold standard for the assessment of lung fibrosis.<sup>9</sup> However, typical animal experiments are laborious and could take months to years to complete. The use of in vitro models can facilitate the rapid

high-throughput assessment of nanomaterial fibrogenicity and disease mechanisms.<sup>10</sup> An important pathological feature of lung fibrosis is the accumulation of ECM that is clinically characterized by fibroblastic foci.<sup>11,12</sup> The presence and extent of such foci is one of the most reliable markers of poor prognosis in patients with fibrosis.<sup>13–15</sup> Xu et al. and Zanotti et al. recently reported an in vitro model using cell clusters (nodules) that resemble the foci of renal and muscle fibrosis.<sup>16,17</sup> In this study, we developed a 3D fibroblastic model of lung fibrosis and investigated the existence of fibroblast-derived fibrogenic stemlike cells (FSCs) and its role in fibrogenesis.

Because fibrosis is a progressive disease associated with aberrant tissue repair and ECM accumulation,<sup>18,19</sup> identifying the cells that are capable of repairing the injured tissue and are the source of ECM production is fundamental to the understanding of fibrosis mechanisms. Evolving research has indicated the presence of putative stem cells to be significant in the development of fibrosis.<sup>20,21</sup> Although the presence of FSCs and its role in fibrogenesis have not been reported, a recent study has indicated the induction of stem cells at the early onset of lung fibrosis in a mouse model of bleomycin-induced fibrosis.<sup>21</sup> Because fibroblasts are known to play a key role in fibrogenesis,<sup>8,22</sup> the present study was undertaken to investigate

**Received:** January 17, 2014

**Revised:** May 19, 2014

**Published:** May 29, 2014

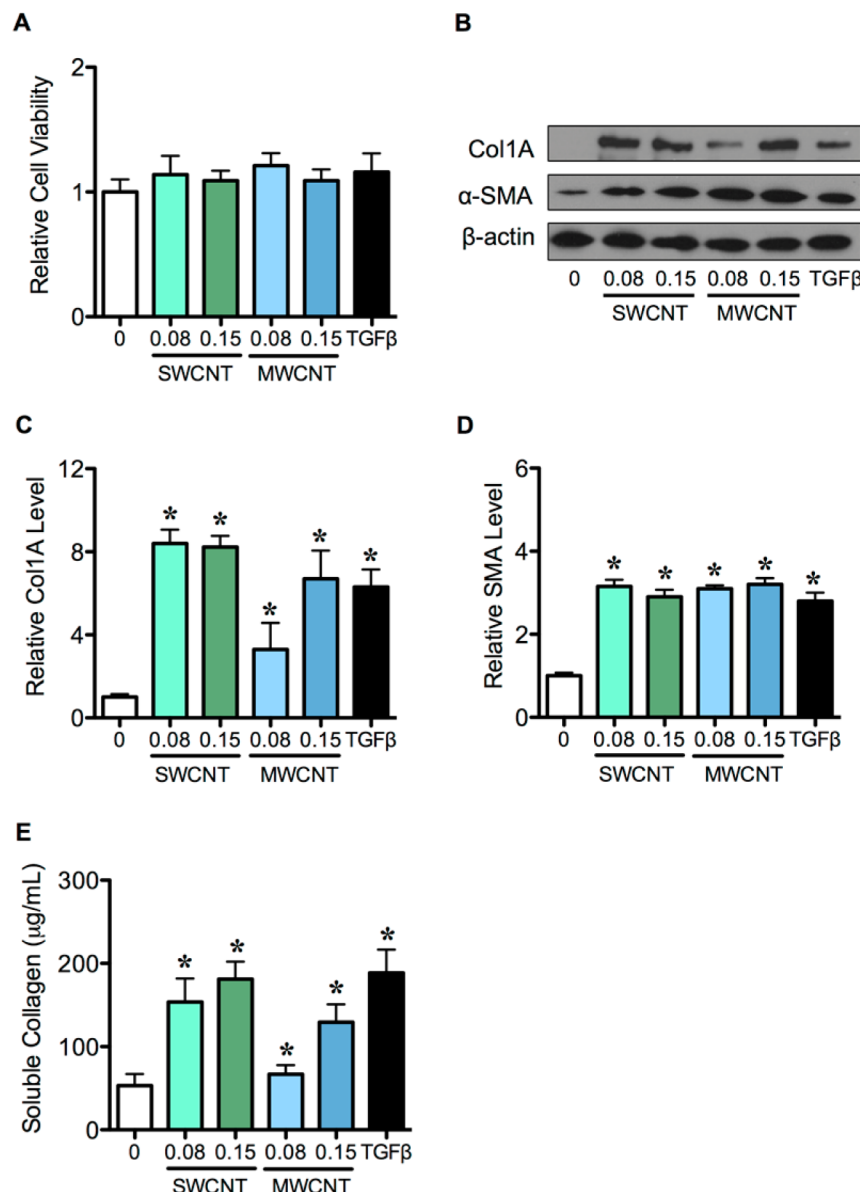


**Figure 1.** Carbon nanotubes induce collagen production of primary human lung fibroblasts. Subconfluent monolayers of cells were treated with various concentrations (0–0.15  $\mu\text{g}/\text{cm}^2$ ) of SWCNT and MWCNT, or TGF- $\beta$  (1 ng/mL) for 48 h. (A) Analysis of cell toxicity and proliferation using MTT assay. (B) Western blot analysis of type I collagen and myofibroblast marker  $\alpha$ -SMA.  $\beta$ -actin was used to confirm equal loading of the samples. (C,D) Quantitative analysis of type I collagen (C) and  $\alpha$ -SMA (D). (E) Soluble collagen content by Sircol assay. Data are mean  $\pm$  SD ( $n = 4$ ). \* $p < 0.05$  versus vehicle-treated control cells.

whether CNT exposure can induce FSCs and whether these cells possess fibrogenic activities. FSCs were induced by exposing primary human lung fibroblasts to CNTs. These cells were used in this study because they are of human origin and a better representation of pathological process than immortalized cell lines that are popularly used but may possess defective genes affecting fibrosis development. Our results demonstrated for the first time the induction of FSCs from normal lung fibroblasts by single-walled (SW) and multiwalled (MW) CNTs. The FSCs possess a high capacity to generate 3D fibroblastic nodules, which were further characterized and assessed as a potential in vitro model for fibrogenicity testing of nanomaterials.

**CNT Characterization and Dose Calculation.** SWCNT were obtained from Carbon Nanotechnology (CNI, Houston, Texas) and were purified by acid treatment to remove metal

contaminates, while MWCNT were obtained from Mitsui & Company (New York, NY). Elemental analysis by nitric acid dissolution and inductive coupled plasma-atomic emission spectrometry (ICP-AES) showed that purified SWCNT and MWCNT contained 99% elemental carbon and less than 1% of contaminants. The metal residues were mostly iron (Fe) at 0.23 and 0.32% by weight in SWCNT and MWCNT, respectively. The BET surface area, length ( $L$ ), and width ( $W$ ) of individual dry CNT were 400–1040  $\text{m}^2/\text{g}$ ,  $0.6 \pm 0.5 \mu\text{m}$  ( $L$ ), and  $1 \pm 0.2 \text{ nm}$  ( $W$ ) for SWCNT, and  $26 \text{ m}^2/\text{g}$ ,  $8.19 \pm 1.7 \mu\text{m}$  ( $L$ ), and  $81 \pm 5 \text{ nm}$  ( $W$ ) for MWCNT.<sup>23,24</sup> CNTs were dispersed by using bovine serum albumin (BSA) and were lightly sonicated prior to culture exposure. The CNT doses used in the in vitro exposure studies were calculated based on in vivo CNT exposure data normalized to alveolar surface area in mice. For example, the doses that induced positive in vivo fibrogenic

response were 40–80  $\mu\text{g}/\text{mouse lung}$  (0.5 mg/kg body weight).<sup>5,6,25</sup> Dividing this dose by the average alveolar surface area in mice ( $\sim 500 \text{ cm}^2$ )<sup>26</sup> indicates the in vitro surface area dose of 0.08–0.16  $\mu\text{g}/\text{cm}^2$ . Extrapolation of the experimental dose to human exposure scenarios in the workplace can be evaluated using the approach adopted by the National Institute for Occupational Safety and Health.<sup>25,27</sup> Assuming the alveolar surface area in humans of  $100 \text{ m}^2$ , the human burden is equal to 80–160 mg/Lung. Considering a lung deposition fraction of 30% and a working day inhalation of  $10 \text{ m}^3$  (a minute ventilation of 20 L/min), the experimental dose could be reached within 3–6 months of human inhalation exposure at  $400 \mu\text{g}/\text{m}^3$  (high CNT level reported in a research facility)<sup>28</sup> or about 10–20 years at  $10 \mu\text{g}/\text{m}^3$  (average CNT level in U.S. facilities)<sup>29</sup> (see Supporting Information Figure S1).

**Effects of CNTs on Cell Growth and Collagen Production of Primary Lung Fibroblasts.** A key cellular mechanism of fibrogenesis is fibroblast activation and subsequent induction of ECM production and accumulation.<sup>30,31</sup> To investigate the effect of CNTs on the fibrogenic process, primary human lung fibroblasts were treated with various concentrations (0–0.15  $\mu\text{g}/\text{cm}^2$  or 0–0.71  $\mu\text{g}/\text{mL}$ ) of SWCNT and MWCNT (see Supporting Information Table S1 for dosimetry) and were evaluated for cell proliferation and collagen production using MTT and Western blot assays. Figure 1A shows that SWCNT and MWCNT had no significant effects on cell proliferation and cytotoxicity at the indicated concentrations, the results that were confirmed by CyQuant cell proliferation assay (Invitrogen, Carlsbad, CA) (data not shown). Figure 1B,C shows that SWCNT, and to a lesser extent MWCNT, strongly induced type I collagen production at the dose as low as  $0.08 \mu\text{g}/\text{cm}^2$ . Transforming growth factor (TGF)- $\beta$ , a known fibrosis inducer that was used in this study as a positive control, similarly induced collagen production at the concentration of 1 ng/mL. Figure 1B,D shows an increased expression of myofibroblast marker  $\alpha$ -smooth muscle actin ( $\alpha$ -SMA) in SWCNT-, MWCNT- and TGF- $\beta$ -treated cells, indicating the transformation of fibroblasts to myofibroblasts, which is known to be the main source of collagen production. Analysis of soluble collagen in the cell culture medium by Sircol assay further showed that both SWCNT and MWCNT induced collagen secretion from the treated cells in a dose-dependent manner (Figure 1E).

**CNTs Induce Fibroblastic Nodule Formation of Primary Lung Fibroblasts.** An important pathological feature of lung fibrosis is the presence of fibroblastic foci, which are aggregates of lung fibroblasts and myofibroblasts and the newly deposited collagen.<sup>11,15</sup> In this study, we developed a 3D biomimetic model of fibroblastic foci by growing primary human lung fibroblasts in culture on an adherent substrate consisting of poly-L-lysine in the presence of TGF- $\beta$ , a known inducer of fibrosis. Figure 2A shows the formation of 3D cell clusters that are referred to as fibroblastic nodules after treatment of the cells with TGF- $\beta$  (1 ng/mL) for 16 h. Interestingly, treatment of the cells with SWCNT or MWCNT similarly induced the fibroblastic nodules, whereas vehicle-treated cells showed minimal nodule formation (Figure 2A). Quantitative analysis for the number of fibroblastic nodules demonstrated the dose-dependent effect of SWCNT and MWCNT treatment (Figure 2B). This number correlates well with the level of collagen produced by the cells as indicated by the correlation plot depicted in Figure 2C showing the linear relationship between the two parameters with a goodness of fit

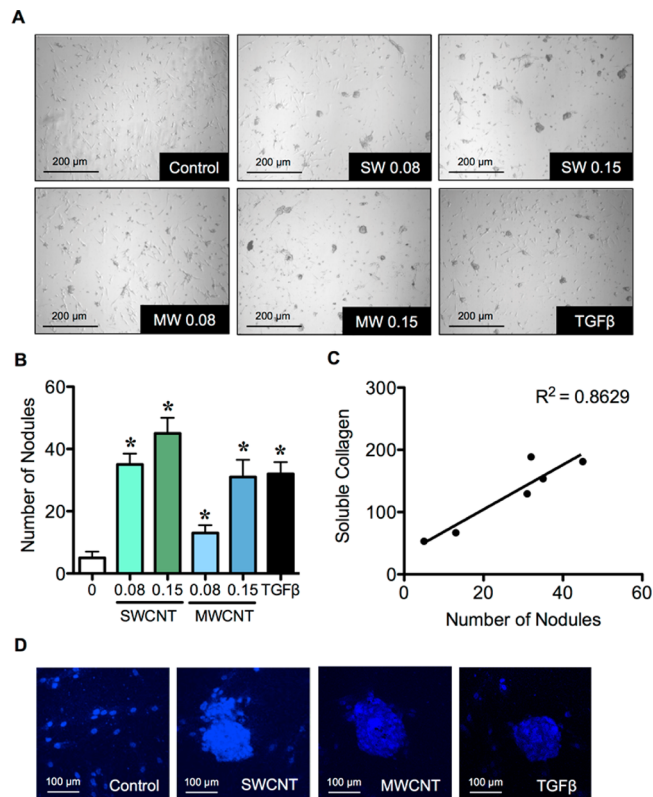


**Figure 2.** Carbon nanotubes induce fibroblastic nodule formation of primary lung fibroblasts. Cells at the density of  $3 \times 10^4$  cells/24-well were grown on a poly-L-lysine-coated glass substrate and treated with various concentrations (0–0.15  $\mu\text{g}/\text{cm}^2$ ) of SWCNT and MWCNT, or TGF- $\beta$  (1 ng/mL) for 16 h, which is the optimal time for fibroblastic formation. (A) Phase contrast micrographs comparing 3D fibroblastic nodules in control and treated fibroblasts. (B) Quantitative analysis of fibroblastic nodules. (C) Correlation analysis of the number of fibroblastic nodules and soluble collagen content. (D) Fluorescence micrographs of fibroblastic nodules induced by SWCNT, MWCNT, and TGF- $\beta$ . Cells were nuclear stained with Hoechst 33342 dye and observed by confocal fluorescence microscopy. Data are mean  $\pm$  SD ( $n = 3$ ). \* $p < 0.05$  versus vehicle-treated control cells.

( $R^2$ ) of 0.8629. To aid visualization of the fibroblastic nodules, the cells were stained with Hoechst 33342 dye and observed under a confocal fluorescence microscope. Figure 2D shows the nodule-forming cell aggregates induced by SWCNT, MWCNT, and TGF- $\beta$  but not by control treatment. The orthogonal views and reconstructed Z-stack image series display 3D morphology of the fibroblastic nodules (Figure 3 and Supporting Information Video S1 and S2). These results support the potential utility of the fibroblastic nodules as an in vitro 3D model for fibrogenicity testing of nanomaterials.

**CNT-Induced Fibroblastic Nodules Contain Abundant Type I Collagen.** Type I collagen is the most abundant ECM proteins robustly expressed in lung fibrosis.<sup>32,33</sup> To further validate the clinical resemblance of the 3D fibroblastic model, type I collagen expression was evaluated in SWCNT-, MWCNT- and TGF- $\beta$ -induced fibroblastic nodules using immunofluorescence in comparison with the monolayer of vehicle-treated control fibroblasts. Figure 4A shows that the fibroblastic nodules induced by CNTs or TGF- $\beta$  were enriched with type I collagen. Together with the cell aggregation data in Figure 2D, we demonstrate here that the fibroblastic nodules have important compositional and morphological features of

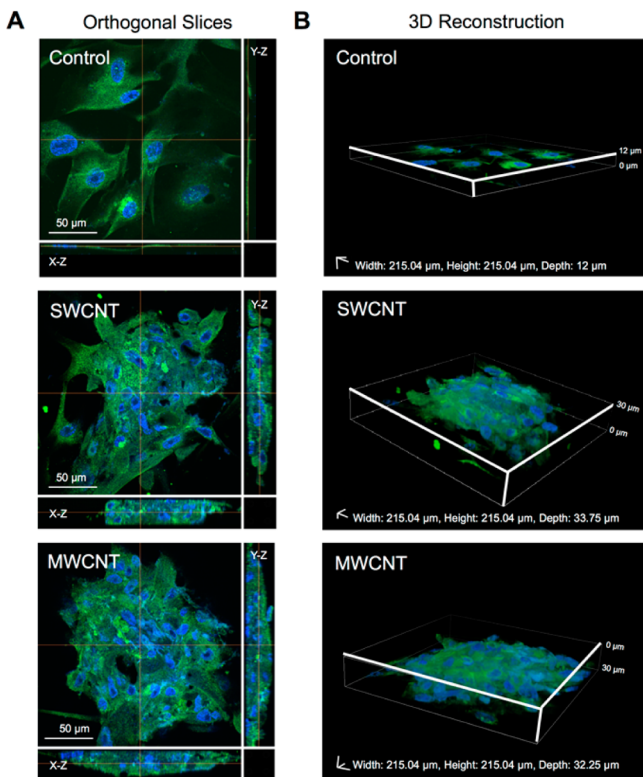


**Figure 3.** Z-stack image series to analyze the 3D structure of fibroblastic nodules. Cells were grown on a poly-L-lysine-coated glass substrate, treated with SWCNT or MWCNT ( $0.15 \mu\text{g}/\text{cm}^2$ ) and immunostained for type I collagen (green) and DAPI-stained for nucleus (blue). (A) X-Y projection of the Z-stack image series from confocal microscopy with the orthogonal views of X-Z plane (bottom) and Y-Z plane (right). (B) Three-dimensional reconstruction was generated based on the results of Z-stack images from panel A. Calibrated dimensions are width ( $215.04 \mu\text{m}$ )  $\times$  height ( $215.04 \mu\text{m}$ )  $\times$  depth (12, 33.75, and  $32.25 \mu\text{m}$ ) in control, SWCNT and MWCNT, respectively.

the fibroblastic foci observed in fibrosis patients. The greater number of fibroblastic nodules in SWCNT as compared to MWCNT (Figure 2) are consistent with previous *in vivo* findings that indicated a greater fibrogenicity of SWCNT than MWCNT,<sup>5,6</sup> thus validating the potential utility of the 3D fibroblastic nodules as a functional assay for CNT fibrogenicity. Overall, the advantages of this 3D model over conventional cell monolayer models include (i) clinical resemblance to human lung fibrotic lesions; (ii) rapid and quantitative or semi-quantitative analysis, that is, by colony (nodule) counting as opposed to the more laborious immunological and biochemical assays; (iii) fewer cell numbers needed per assay; and (iv) potential for high-throughput screening, that is, by using automated colony counter.

**CNT-Induced Fibroblastic Nodules Express a High Level of Putative Stem Cell Markers.** Evolving research indicates the presence of putative stem cells residing in the lungs to be significant in an early development of lung fibrosis.<sup>21</sup> To investigate the existence of stemlike fibroblasts, we performed immunofluorescence assays determining the expression of universal stem cell markers ABCG2 and ALDH1A1<sup>34,35</sup> in fibroblastic nodules induced by SWCNT, MWCNT, and TGF- $\beta$ . Figure 4B shows that these fibroblastic nodules expressed a high level of ABCG2 and ALDH1A1 stem cell markers as compared to vehicle-treated control cells. These

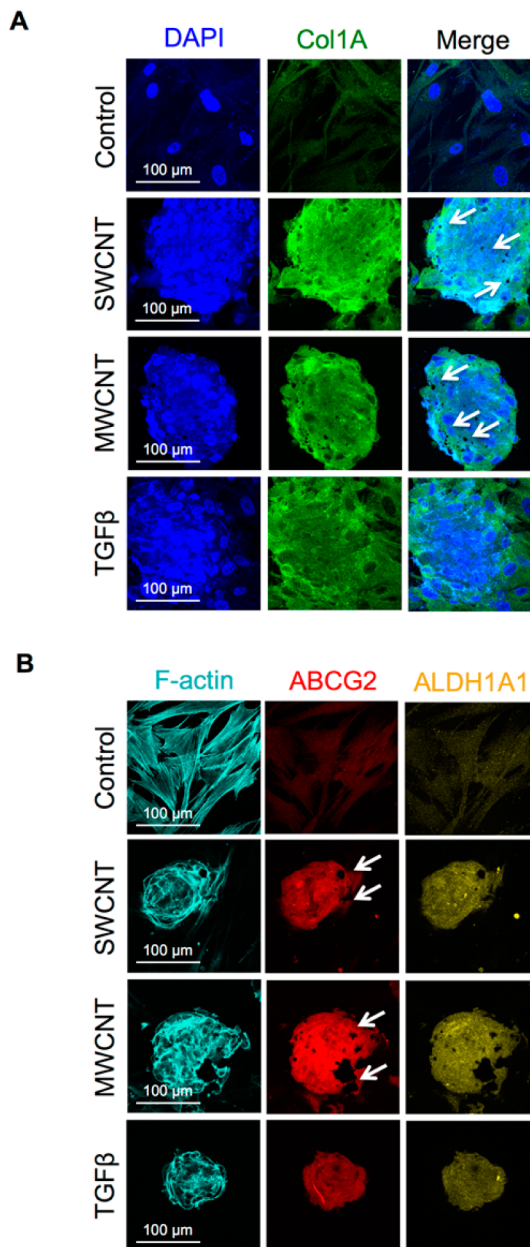


**Figure 4.** Expression of type I collagen and stem cell markers in carbon nanotube-induced fibroblastic nodules. Cells were grown on a poly-L-lysine-coated substrate and treated with SWCNT ( $0.15 \mu\text{g}/\text{cm}^2$ ), MWCNT ( $0.15 \mu\text{g}/\text{cm}^2$ ), or TGF- $\beta$  ( $1 \text{ ng}/\text{mL}$ ) for 16 h. (A) Fluorescence micrographs of control and fibroblastic nodules induced by CNTs and TGF- $\beta$  immunostained for type I collagen (green) and DAPI-stained for nucleus (blue) by confocal fluorescence microscopy. (B) Fluorescence micrographs of control and fibroblastic nodules immunostained for stem cell surface markers ABCG2 (red) and ALDH1A1 (yellow) by confocal fluorescence microscopy.

results suggest the presence of stemlike cells in the fibroblastic nodules and support their role in fibrogenesis. We also observed CNT deposition in the fibroblastic nodules induced by SWCNT and MWCNT (Figure 4A and B, arrows) with minimal presence of CNTs outside the nodules.

**CNTs Induce Side Population Phenotype of Primary Lung Fibroblasts.** Adult stem cells are known to efflux Hoechst dye slowly due to the high expression of ABCG2. Flow cytometric analysis was used to identify these stem cells with a

distinct low Hoechst staining pattern referred to as side population (SP).<sup>36,37</sup> An increase in SP population was reported in the lung of mice with fibrosis, suggesting the involvement of SP-positive stem cells in lung fibrogenesis.<sup>21</sup> To determine the potential role of stemlike fibroblasts in CNT-induced fibrogenesis, we first determined the change of SP subpopulation upon CNT treatment. Primary human lung fibroblasts were treated with SWCNT or MWCNT at the concentration of  $0.15 \mu\text{g}/\text{cm}^2$  for 48 h, after which they were incubated with  $5 \mu\text{g}/\text{mL}$  of Hoechst 33342 in the presence or absence of  $25 \mu\text{M}$  fumitremorgin C, an inhibitor of ABC transporter. Figure 5A shows that both SWCNT and MWCNT were able to induce the SP subpopulation. The percentage of SP was approximately 5% in SWCNT-treated fibroblasts and 3% in MWCNT-treated cells versus less than 0.5% in vehicle-treated control cells (Figure 5B).

**Increased Stem Cell Marker and Collagen Expression in CNT-Derived SP Fibroblasts.** To determine the role of

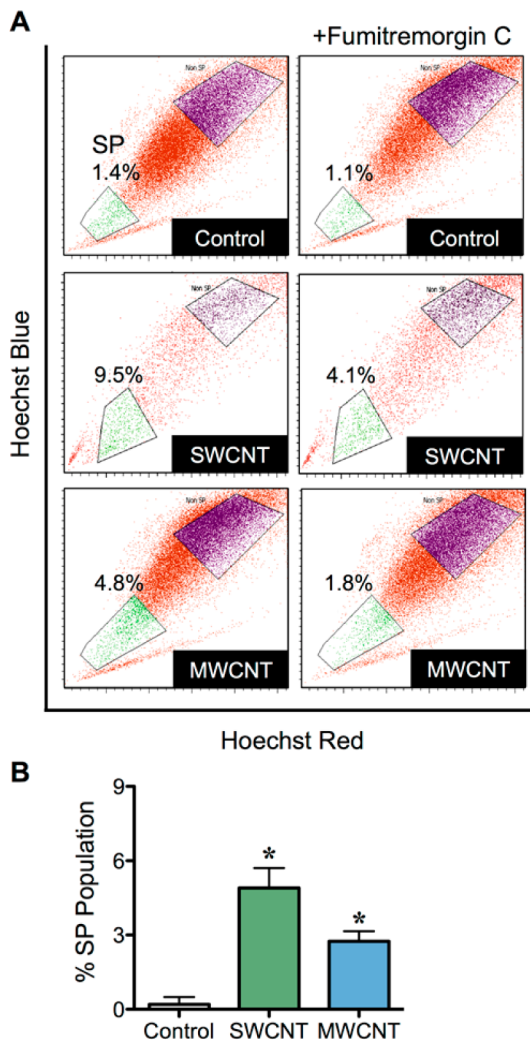


**Figure 5.** Carbon nanotubes induce stemlike cells as indicated by side population phenotype. Fibroblasts were treated with SWCNT ( $0.15 \mu\text{g}/\text{cm}^2$ ) or MWCNT ( $0.15 \mu\text{g}/\text{cm}^2$ ) for 48 h. (A) Analysis of side population (SP) in vehicle- and CNT-treated cells in the presence or absence of fumitremorgin c (FTC) using FACS. SP cells (box) are determined by their disappearance in the presence of FTC. (B) Quantitative analysis of SP subpopulation. Data are mean  $\pm$  SD ( $n = 4$ ). \* $p < 0.05$  versus vehicle-treated control cells.

stemlike fibroblasts in CNT-induced fibrogenesis, we isolated the stemlike cells from SWCNT-treated ( $0.15 \mu\text{g}/\text{cm}^2$ ) fibroblasts based on their SP phenotype using fluorescence-activated (flow cytometry-based) cell sorting (FACS). Sorted SP and non-SP fibroblasts were further evaluated for the stem cell marker ABCG2 and type I collagen expression by immunofluorescence. Figure 6A,B reveals a substantially higher

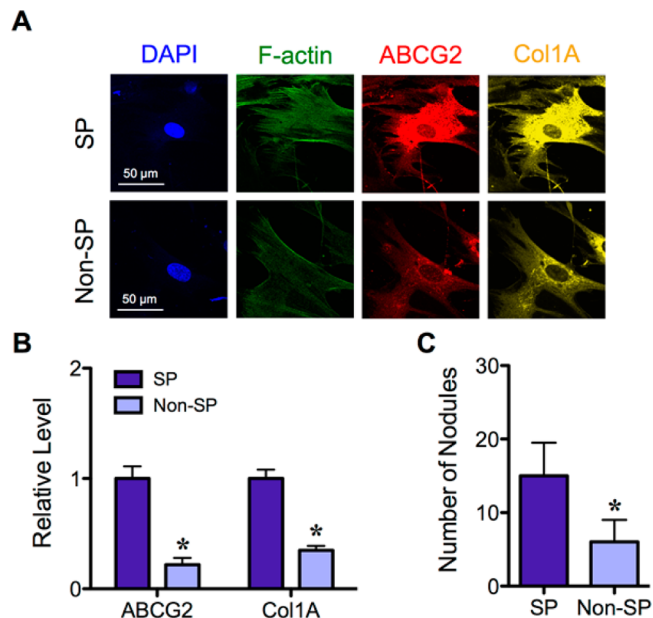


**Figure 6.** An enhanced fibrogenic activity of carbon nanotube-derived SP fibroblasts. Cells were treated with SWCNT ( $0.15 \mu\text{g}/\text{cm}^2$ ) or MWCNT ( $0.15 \mu\text{g}/\text{cm}^2$ ) for 48 h and stained with Hoechst 33342 dye for side population (SP) analysis. SP fibroblasts were characterized and isolated by FACS. (A) Fluorescence micrographs of the sorted SP fibroblasts and parental control non-SP fibroblasts immunostained for phalloidin (F-actin, green), stem cell marker ABCG2 (red), and type I collagen (yellow) by confocal fluorescence microscopy. (B) Quantitative analysis of ABCG2 and type I collagen expression. (C) Sorted SP and non-SP fibroblasts were grown on a poly-L-lysine-coated substrate, treated with SWCNT ( $0.15 \mu\text{g}/\text{cm}^2$ ), and analyzed for fibroblastic nodule formation at 16 h post-treatment. Data are mean  $\pm$  SD ( $n = 3$ ). \* $p < 0.05$  versus SP fibroblasts.

expression of ABCG2 in the SP versus non-SP cells, thus confirming the stemlike phenotype of SP fibroblasts and the reliability of stem cell isolation by FACS. Importantly, type I collagen expression was significantly higher in the SP versus non-SP population. It is widely known that fibroblasts play a key role in fibrogenesis through its ability to synthesize and secrete ECM proteins including type I collagen, which characterizes fibrosis.<sup>38,39</sup> Our results thus indicate that the stemlike fibroblasts are a potential key source of collagen production and may play a crucial role in fibrogenesis.

**CNT-Derived SP Fibroblasts Are Potent Inducer of Fibroblastic Nodules.** To substantiate the functional role of stem-like fibroblasts in CNT fibrogenesis, the sorted SP and non-SP cells from CNT-treated fibroblasts were assessed for their ability to form fibroblastic nodules. Figure 6C shows that that SP cells had a substantially higher capability to form fibroblastic nodules than the non-SP fibroblasts. Altogether, these findings support the role of stemlike fibroblasts in CNT-induced fibrogenesis.

**Expression of Stem Cell Markers in Human Lung Fibrosis Tissues.** To provide a supporting evidence for the clinical relevance of stem cells in lung fibrosis, we performed an expression analysis of universal stem cell markers ALDH1A1 and ABCG2 in human clinical specimens from fibrotic and matched normal lung tissues (Origene, Rockville, MD) using immunohistochemistry and immunofluorescence, respectively. Figure 7A demonstrates for the first time an upregulation of the

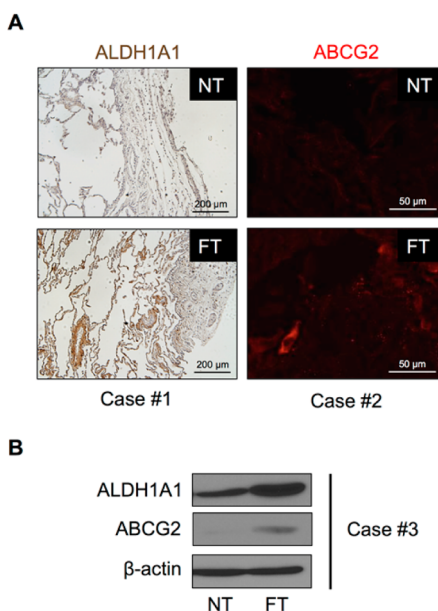


**Figure 7.** Expression analysis of stem cell markers ALDH1A1 and ABCG2 in human lung fibrosis tissues. (A) Left: Immunohistochemistry staining for ALDH1A1 expression in formalin-fixed, paraffin-embedded human lung specimens from fibrotic tissues (FT) and matched normal tissues (NT). Right: Immunofluorescence staining for ABCG2 expression in lung fibrotic and matched normal frozen tissues. (B) Western blot analysis of ALDH1A1 and ABCG2 expression in protein lysates from fibrotic and matched normal lung tissues.

stem cell markers in human lung fibrosis tissues as compared to matched normal lung tissues. Quantitative analysis of the stem cell marker expression by Western blotting further showed an increased expression of ALDH1A1 and ABCG2 in the cell lysates obtained from lung fibrosis tissues versus matched normal lung tissues (Figure 7B). These data provide preliminary supporting evidence for the role of stem cells in human lung fibrosis. As the high expression of ALDH1A1 and ABCG2 was similarly observed in the CNT-fibrotic nodules, these findings strengthen the role of stemlike fibroblasts in CNT-induced fibrogenesis.

In summary, we have developed a 3D model of CNT lung fibrogenesis that is fast, robust, and resembles the clinical fibrotic foci of lung fibrosis. The model employs primary human lung fibroblasts that form a collagen-rich 3D structure upon stimulation with CNTs or TGF- $\beta$ . Using this model, we unveiled the presence of fibroblast stemlike cells in the fibroblastic nodules and demonstrated its role in CNT-induced fibrogenesis. The developed model could potentially be used as an alternative assay to predict the fibrogenicity of CNTs and other nanomaterials for their safer design and risk assessment. In addition, the model could be used to aid mechanistic investigations of the cellular and molecular events leading to fibrogenesis.

## ■ ASSOCIATED CONTENT

### ● Supporting Information

Supplementary Figure S1: Extrapolation of the carbon nanotube experimental dose in mouse and cell culture models to human exposure scenarios in the workplace. Supplementary Table S1: In vitro dosimetry of carbon nanotubes. Supplementary Video S1: Three-dimensional reconstruction of Z-stack confocal image series of fibroblastic nodules induced by SWCNT. Supplementary Video S2: Three-dimensional reconstruction of Z-stack confocal image series of fibroblastic nodules induced by MWCNT. Supplementary materials and methods. This material is available free of charge via the Internet at <http://pubs.acs.org>.

## ■ AUTHOR INFORMATION

### Corresponding Author

\*E-mail: yrojan@hsc.wvu.edu. Phone: 304- 293-1476.

### Author Contributions

The manuscript was written through contributions of all authors. All authors have given approval to the final version of the manuscript.

### Notes

The authors declare no competing financial interest.

## ■ ACKNOWLEDGMENTS

This work was supported by the National Institute for Occupational Safety and Health and by grants from the National Institutes of Health (NIH; R01-HL095579 and R01-ES022968) and National Science Foundation (EPS-1003907). Flow cytometric analysis was performed in the West Virginia University Flow Cytometry Core Facility, which is supported in part by the NIH Grant P30 GM103488. Imaging experiments and image analysis were performed in the West Virginia University Microscope Imaging Facility, which has been supported by the Mary Babb Randolph Cancer Center and NIH Grants P20 RR016440, P30 RR032138/GM103488, and P20 RR016477. The authors also thank Jingting Li for her excellent technical assistance. The findings and conclusions in this report are those of the authors and do not necessarily represent the views of the National Institute for Occupational Safety and Health.

## ■ ABBREVIATIONS

CNT, carbon nanotube; SWCNT, single-walled CNT; MWCNT, multiwalled CNT; TGF- $\beta$ , transforming growth factor beta; 3D, three-dimensional; SP, side population; ECM, extracellular matrix; FACS, fluorescence-activated (flow cytometry-based) cell sorting; FSC, fibroblast stemlike cell

## ■ REFERENCES

- (1) Shvedova, A. A.; Kisin, E. R.; Porter, D.; Schulte, P.; Kagan, V. E.; Fadeel, B.; Castranova, V. *Pharmacol. Ther.* **2009**, *121*, 192–204.
- (2) Helland, A.; Wick, P.; Koehler, A.; Schmid, K.; Som, C. *Environ. Health Perspect.* **2007**, *115*, 1125–1131.
- (3) Snyder-Talkington, B. N.; Schwegler-Berry, D.; Castranova, V.; Qian, Y.; Guo, N. L. *Part. Fibre Toxicol.* **2013**, *10*, 35.
- (4) Shvedova, A. A.; Kisin, E. R.; Mercer, R.; Murray, A. R.; Johnson, V. J.; Potapovich, A. I.; Tyurina, Y. Y.; Gorelik, O.; Arepalli, S.; Schwegler-Berry, D.; et al. *Am. J. Physiol.: Lung Cell. Mol. Physiol.* **2005**, *289*, L698–L707.
- (5) Mercer, R. R.; Scabilloni, J.; Wang, L.; Kisin, E.; Murray, A. R.; Schwegler-Berry, D.; Shvedova, A. A.; Castranova, V. *Am. J. Physiol.: Lung Cell. Mol. Physiol.* **2008**, *294*, L87–97.

- (6) Mercer, R. R.; Hubbs, A. F.; Scabilloni, J. F.; Wang, L.; Battelli, L. A.; Friend, S.; Castranova, V.; Porter, D. W. *Part. Fibre Toxicol.* **2011**, *8*, 21.
- (7) Wang, L.; Castranova, V.; Mishra, A.; Chen, B.; Mercer, R. R.; Schwegler-Berry, D.; Rojanasakul, Y. *Part. Fibre Toxicol.* **2010**, *7*, 31–41.
- (8) Wang, L.; Mercer, R. R.; Rojanasakul, Y.; Qiu, A.; Lu, Y.; Scabilloni, J. F.; Wu, N.; Castranova, V. *J. Toxicol. Environ. Health, Part A* **2010**, *73*, 410–422.
- (9) Nel, A.; Xia, T.; Meng, H.; Wang, X.; Lin, S.; Ji, Z.; Zhang, H. *Acc. Chem. Res.* **2013**, *46*, 607–621.
- (10) Moore, B. B.; Lawson, W. E.; Oury, T. D.; Sisson, T. H.; Raghavendran, K.; Hogaboam, C. M. *Am. J. Respir. Cell Mol. Biol.* **2013**, *49*, 167–179.
- (11) Cha, S. I.; Groshong, S. D.; Frankel, S. K.; Edelman, B. L.; Cosgrove, G. P.; Terry-Powers, J. L.; Remigio, L. K.; Curran-Everett, D.; Brown, K. K.; Cool, C. D.; et al. *Am. J. Respir. Cell Mol. Biol.* **2010**, *42*, 140–148.
- (12) Harada, T.; Watanabe, K.; Nabeshima, K.; Hamasaki, M.; Iwasaki, H. *Respirology* **2013**, *18*, 278–283.
- (13) Meuten, T.; Hickey, A.; Franklin, K.; Grossi, B.; Tobias, J.; Newman, D. R.; Jennings, S. H.; Correa, M.; Sannes, P. L. *Respir. Res.* **2012**, *13*, 62.
- (14) Lomas, N. J.; Watts, K. L.; Akram, K. M.; Forsyth, N. R.; Spiteri, M. A. *Int. J. Clin. Exp. Pathol.* **2012**, *5*, 58–71.
- (15) Liu, G.; Friggeri, A.; Yang, Y.; Milosevic, J.; Ding, Q.; Thannickal, V. J.; Kaminski, N.; Abraham, E. J. *Exp. Med.* **2010**, *207*, 1589–1597.
- (16) Xu, Q.; Norman, J. T.; Shrivastav, S.; Lucio-Cazana, J.; Kopp, J. B. *Am. J. Physiol. Renal Physiol.* **2007**, *293*, F631–F640.
- (17) Zanotti, S.; Gibertini, S.; Savadori, P.; Mantegazza, R.; Mora, M. *Cell Tissue Res.* **2013**, *352*, 659–70.
- (18) Bonniaud, P.; Margetts, P. J.; Kolb, M.; Schroeder, J. A.; Kapoun, A. M.; Damm, D.; Murphy, A.; Chakravarty, S.; Dugar, S.; Higgins, L.; Protter, A. A.; et al. *Am. J. Respir. Crit. Care Med.* **2005**, *171*, 889–898.
- (19) Leask, A.; Abraham, D. J. *FASEB J.* **2004**, *18*, 816–827.
- (20) Lebleu, V. S.; Taduri, G.; O'Connell, J.; Teng, Y.; Cooke, V. G.; Woda, C.; Sugimoto, H.; Kalluri, R. *Nat. Med.* **2013**, *19*, 1047–1053.
- (21) Banerjee, E. R.; Henderson, W. R., Jr. *Stem Cell Res. Ther.* **2012**, *3*, 21.
- (22) Mishra, A.; Rojanasakul, Y.; Chen, B. T.; Castranova, V.; Mercer, R. R.; Wang, L. *J. Nanomater.* **2012**, *2012*, 930931.
- (23) Wang, L.; Luanpitpong, S.; Castranova, V.; Tse, W.; Lu, Y.; Pongrakhananon, V.; Rojanasakul, Y. *Nano Lett.* **2011**, *11*, 2796–2803.
- (24) Wang, L.; Stueckle, T.; Mishra, A.; Derk, R.; Meighan, T.; Castranova, V.; Rojanasakul, Y. *Nanotoxicology* **2014**, *8*, 485–507.
- (25) Porter, D. W.; Hubbs, A. F.; Mercer, R. R.; Wu, N.; Wolfarth, M. G.; Sriram, K.; Leonard, S.; Battelli, L.; Schwegler-Berry, D.; Friend, S.; et al. *Toxicology* **2010**, *269*, 136–147.
- (26) Stone, K. C.; Mercer, R. R.; Gehr, P.; Stockstill, B.; Crapo, J. D. *Am. J. Respir. Cell Mol. Biol.* **1992**, *6*, 235–243.
- (27) Vietti, G.; Ibouaraadaten, S.; Palmai-Pallag, M.; Yahoub, Y.; Bailly, C.; Fenoglio, I.; Marbaix, E.; Lison, D.; van den Brule, S. *Part. Fibre Toxicol.* **2013**, *10*, 52.
- (28) Han, J. H.; Lee, E. J.; Lee, J. H.; So, K. P.; Lee, Y. H.; Bae, G. N.; Lee, S. B.; Ji, J. H.; Cho, M. H.; Yu, I. *J. Inhal. Toxicol.* **2008**, *20*, 741–749.
- (29) Erdely, A.; Dahm, M.; Chen, B. T.; Zeidler-Erdely, P. C.; Fernback, J. E.; Birch, M. E.; Evans, D. E.; Kashon, M. L.; Deddens, J. A.; Hulderman, T.; et al. *Part. Fibre Toxicol.* **2013**, *10*, 53.
- (30) Raghu, G.; Chen, Y. Y.; Rusch, V.; Rabinovitch, P. S. *Am. Rev. Respir. Dis.* **1988**, *138*, 703–708.
- (31) Pechkovsky, D. V.; Prasse, A.; Kollert, F.; Engel, K. M.; Dentler, J.; Luttmann, W.; Friedrich, K.; Müller-Quernheim, J.; Zissel, G. *Clin. Immunol.* **2010**, *137*, 89–101.
- (32) Nho, R. S. *Clin. Res. Pulmonol.* **2013**, *1*, 1008.
- (33) Cox, T. R.; Erler, J. T. *Dis. Models & Mech.* **2011**, *4*, 165–178.
- (34) Ding, X. W.; Wu, J. H.; Jiang, C. P. *Life Sci.* **2010**, *86*, 631–637.
- (35) Douville, J.; Beaulieu, R.; Balicki, D. *Stem Cells Dev.* **2009**, *18*, 17–26.
- (36) Majka, S. M.; Beutz, M. A.; Hagen, M.; Izzo, A. A.; Voelkel, N.; Helm, K. M. *Stem Cells* **2005**, *23*, 1073–1081.
- (37) Golebiewska, A.; Brons, N. H. C.; Bjerkvig, R.; Niclou, S. P. *Cell Stem Cell* **2011**, *8*, 136–147.
- (38) Ramos, C.; Montano, M.; Garcia-Alvarez, J.; Ruiz, V.; Uhal, B. D.; Selman, M.; Pardo, A. *Am. J. Respir. Cell Mol. Biol.* **2011**, *24*, 591–598.
- (39) Fan, D.; Takawale, A.; Lee, J.; Kassiri, Z. *Fibrog. Tissue Repair* **2012**, *5*, 15.